The Store-operated Calcium Entry Pathways in Human Carcinoma A431 Cells: Functional Properties and Activation Mechanisms

Konstantin Gusev,[1] Lyuba Glouchankova,[1] Alexander Zubov,[1] Elena Kaznacheyeva,[1] Zhengnan Wang,[2] Ilya Bezprozvanny,[2] and Galina N. Mozhayeva[1]

[1]Institute of Cytology RAS, St. Petersburg 194064, Russia

[2]Department of Physiology, University of Texas Southwestern Medical Center at Dallas, Dallas, TX 75390

ABSTRACT Activation of phospholipase C (PLC)-mediated signaling pathways in nonexcitable cells causes the release of Ca^{2+} from intracellular Ca^{2+} stores and activation of Ca^{2+} influx across the plasma membrane. Two types of Ca^{2+} channels, highly Ca^{2+}–selective I_{CRAC} and moderately Ca^{2+}–selective I_{SOC}, support store-operated Ca^{2+} entry process. In previous patch-clamp experiments with a human carcinoma A431 cell line we described store-operated I_{min}/I_{CRACL} plasma membrane Ca^{2+} influx channels. In the present paper we use whole-cell and single-channel recordings to further characterize store-operated Ca^{2+} influx pathways in A431 cells. We discovered that (a) I_{CRAC} and I_{SOC} are present in A431 cells; (b) I_{CRAC} currents are highly selective for divalent cations and fully activate within 150 s after initiation of Ca^{2+} store depletion; (c) I_{SOC} currents are moderately selective for divalent cations (P_{Ba}/P_{Cs} = 14.5) and require at least 300 s for full activation; (d) I_{CRAC} and I_{SOC} currents are activated by PLC-coupled receptor agonists; (e) I_{SOC} currents are supported by I_{min}/I_{CRACL} channels that display 8.5–10 pS conductance for sodium; (f) I_{CRAC} single channel conductance for sodium is estimated at 0.9 pS by the noise analysis; (g) I_{min}/I_{CRACL} channels are activated in excised patches by an amino-terminal fragment of $InsP_3R1$ ($InsP_3R1N$); and (h) $InsP_3$ binding to $InsP_3R1N$ is necessary for activation of I_{min}/I_{CRACL} channels. Our findings provide novel information about store-operated Ca^{2+} influx pathways in A431 cells.

KEY WORDS: calcium signaling • patch-clamp • inositol 1,4,5-trisphosphate • calcium channels • whole-cell

INTRODUCTION

Activation of PLC-mediated signaling pathways in nonexcitable cells causes the release of Ca^{2+} from intracellular Ca^{2+} stores and promotes Ca^{2+} influx across the plasma membrane via capacitative Ca^{2+} entry (CCE)* or store-operated Ca^{2+} entry (SOC) processes (Berridge, 1995; Parekh and Penner, 1997; Putney et al., 2001; Venkatachalam et al., 2002). Two types of Ca^{2+} channels have been implicated in store-operated Ca^{2+} entry in nonexcitable cells. Highly Ca^{2+}-selective channels ($P_{D/M} > 1{,}000$) named "Ca^{2+} release activated channels" (I_{CRAC}) have been initially discovered in studies of Jurkat and RBL cells (Hoth and Penner, 1992; Zweifach and Lewis, 1993; Premack et al., 1994). Moderately Ca^{2+}-selective channels have been later identified in a number of cells and grouped under the name I_{SOC} (Berridge, 1995; Parekh and Penner, 1997; Nilius and Droogmans, 2001; Putney et al., 2001; Venkatachalam et al., 2002). When compared with I_{CRAC}, I_{SOC} channels display lower selectivity for divalent cations ($P_{D/M} \sim 10$), at least 10-fold higher single channel conductance for divalent and monovalent cations, and different kinetic and pharmacological properties (Berridge, 1995; Parekh and Penner, 1997; Nilius and Droogmans, 2001; Putney et al., 2001; Venkatachalam et al., 2002). The molecular identity of I_{CRAC} remains unclear (Clapham, 1996; Parekh and Penner, 1997; Putney et al., 2001; Venkatachalam et al., 2002). Mammalian *trp* channels of TRPC family are the most likely candidates for the role of I_{SOC} channels (Birnbaumer et al., 1996; Clapham et al., 2001; Nilius and Droogmans, 2001; Montell et al., 2002; Venkatachalam et al., 2002; Zitt et al., 2002).

The mechanisms of I_{SOC} and I_{CRAC} channel activation have been under intense investigation (Birnbaumer et al., 1996; Clapham et al., 2001; Nilius and Droogmans, 2001; Montell et al., 2002; Venkatachalam et al., 2002; Zitt et al., 2002). Activation of I_{SOC}/I_{CRAC} channels by a diffusible messenger CIF (Ca^{2+}-influx factor) released by depleted Ca^{2+} stores (Putney and Bird, 1993; Randriamampita and Tsien, 1993; Kim et al., 1995; Csutora et al., 1999; Trepakova et al., 2000), via "conformational coupling" with the intracellular $InsP_3R$ (Irvine, 1990; Kiselyov et al., 1998; Zubov et al., 1999), by cleavage of PIP_2 (Kaznacheyeva et al., 2000; Estacion et al., 2001), and by regulated insertion of channels into plasma membrane (Patterson et al., 1999; Yao et al., 1999) have been considered. Direct association of

Address correspondence to Dr. Ilya Bezprozvanny, Department of Physiology, K4.112, UT Southwestern Medical Center at Dallas, 5323 Harry Hines Blvd., Dallas, TX 75390-9040. Fax: (214) 648-2974; E-mail: Ilya.Bezprozvanny@UTSouthwestern.edu

*Abbreviations used in this paper: CCE, Ca^{2+} entry; DVF, divalent-free; SOC, store-operated Ca^{2+} entry.

J. Gen. Physiol. © The Rockefeller University Press • 0022-1295/2003/07/81/14 $8.00
Volume 122 July 2003 81–94
http://www.jgp.org/cgi/doi/10.1085/jgp.200308815

TrpC3 and TrpC4 with the $InsP_3R$ amino terminus (Boulay et al., 1999; Tang et al., 2001) provided a biochemical support to conformational-coupling model of I_{SOC} activation. The mechanisms of I_{CRAC} activation remain poorly understood.

In experiments with a human carcinoma A431 cell line we previously described I_{min} plasma membrane Ca^{2+} channels that are activated by application of uridine triphosphate and bradykinin to cell-attached patches or by application of $InsP_3$ to excised inside-out patches (Kiselyov et al., 1997, 1999b; Mozhayeva et al., 1990). We found that major functional properties of I_{min} channels, such as small conductance (1–1.5 pS for divalent cations) and sensitivity to block by SKF95365 are similar to I_{CRAC} channels (Kiselyov et al., 1999b; Zubov et al., 1999). We further demonstrated that activation of I_{min} channels by $InsP_3$ in inside-out patches is facilitated by anti-PIP_2 antibodies and suggested a $InsP_3R$–PIP_2–I_{min} signaling complex in these cells (Kaznacheyeva et al., 2000). More recently we demonstrated activation of I_{min} channels in A431 cells by depletion of intracellular Ca^{2+} stores and renamed these channels I_{CRACL} (I_{CRAC}-like) (Kaznacheyeva et al., 2001).

Our previous characterization of I_{min}/I_{CRACL} channels in A431 cells was performed at the single-channel level by patch-clamp technique (Mozhayeva et al., 1990; Kiselyov et al., 1997, 1999b; Kaznacheyeva et al., 2000, 2001; Zubov et al., 1999). In these experiments we determined that the monovalent single-channel conductance of I_{min}/I_{CRACL} channels is in the range 8.5–10 pS (Kaznacheyeva et al., 2001). The I_{CRAC} channels were described in Jurkat and RBL cells in whole-cell recordings (Hoth and Penner, 1992; Zweifach and Lewis, 1993; Premack et al., 1994) and the channels with 40 pS conductance for monovalent cations had been measured in Jurkat cells (Kerschbaum and Cahalan, 1999). Recently, Mg^{2+} and ATP-sensitive I_{MagNuM} (Mg^{2+}- and nucleotide-regulated metal) channels encoded by TRPM7 were described in RBL and Jurkat cells (Nadler et al., 2001; Runnels et al., 2001; Hermosura et al., 2002). Channels with identical properties were also uncovered in RBL and Jurkat cells by other groups and called I_{MIC} (Mg^{2+}-inhibited channels) (Kozak et al., 2002; Prakriya and Lewis, 2002). It appears that TRPM7 protein encodes both I_{MagNuM} and I_{MIC} channels, and in our paper we will use the originally proposed I_{MagNuM} nomenclature (Nadler et al., 2001). I_{MagNuM} channels display 40 pS conductance for monovalent cations (Prakriya and Lewis, 2002), and it appears that the previously measured 40 pS channels present in Jurkat cells (Kerschbaum and Cahalan, 1999) correspond to I_{MagNuM}, not to I_{CRAC} (Kozak et al., 2002). In fact, recent noise measurements suggested that the monovalent conductance of I_{CRAC} channels in Jurkat cells is no more than 0.2 pS (Prakriya and Lewis, 2002).

These results pose a number of questions. What is a relationship between I_{CRAC}, I_{SOC}, I_{MagNuM}, and I_{min}/I_{CRACL} channels in A431 cells? What is a mechanism of I_{min}/I_{CRACL} activation? To answer these questions, we analyzed store-operated Ca^{2+} influx pathways in A431 cells by whole-cell and single-channel recordings. We discovered that both I_{min}/I_{CRACL} and I_{CRAC} channels are activated by intracellular Ca^{2+} store-depletion, by cytosolic $InsP_3$, and by PLC-linked agonists. However, I_{CRAC} channels are activated by Ca^{2+} store-depletion faster than I_{min}/I_{CRACL} channels and are more selective for divalent cations than I_{min}/I_{CRACL} channels. In some experiments we also observed channels with the properties typical of I_{MagNuM} (Clapham, 2002; Hermosura et al., 2002; Kozak et al., 2002; Prakriya and Lewis, 2002). These channels were clearly distinct from I_{min}/I_{CRACL} channels. Thus, we concluded that I_{min}/I_{CRACL} channels correspond to I_{SOC} and not to I_{CRAC} or I_{MagNuM} channels in A431 cells. In additional experiments we demonstrated activation of I_{min}/I_{CRACL} channels by the amino-terminal recombinant fragment of $InsP_3R1$, in support of a conformational coupling activation model of I_{SOC} in A431 cells.

MATERIALS AND METHODS

Cells

Human carcinoma A431 cells (Cell Culture Collection) were kept in culture as described elsewhere (Kiselyov et al., 1999b). For patch clamp experiments cells were seeded onto coverslips and maintained in culture for 1 to 3 d before use.

Electrophysiology

All electrophysiological experiments were performed using a PC-501A patch clamp amplifier (Warner Instruments) with a conventional 10 GΩ feed-back resistance in the head stage. Resistance of sylgard-coated, fire-polished glass microelectrodes varied from 3 to 5 MΩ. Series resistance was not compensated. During recording the currents were sampled at 2.5 kHz and filtered digitally at 500 Hz. In all whole-cell experiments the holding potential was 0 mV. Periodically (once every 4–30 s) the membrane potential was stepped to −100 mV (for 30 ms) and a 170 ms voltage ramp to 70 mV was applied. Traces recorded before I_{CRAC} and I_{SOC} current activation were used as a template for leak subtraction. The recorded currents were normalized to the cell capacitance. Mean value of cell capacitance was 25 ± 2 pF (n = 36). The current reversal potential (E_{rev}) was corrected by a 5.9 mV liquid-junction potential (Barry, 1994) in calculations of P_{Ba}/P_{Cs} permeability ratio. To calculate P_{Ba}/P_{Cs} permeability ratio we used GHK equation (Hille, 2001):

$$P_{Ba}/P_{Cs} = [A_{Cs}/4A_{Ba}]\exp(E_{rev}F/RT)[(E_{rev}F/RT) + 1], \quad (1)$$

where $A_{Cs} = \gamma_{Cs}[Cs]_{in}$ and $A_{Ba} = \gamma_{Ba}[Ba]_o$; $\gamma_{Cs} = 0.82$ and $\gamma_{Ba} = 0.46$.

Single channel recordings data were collected from 10-s records at the given membrane potential (between −90 and −10 mV), digitized at 2.5 kHz and filtered at 100 Hz for analysis and presentation. Unitary current amplitude was determined from current records and all-point amplitude histograms. The experiments were performed at room temperature (22–24°C). Data are

given as mean ± SE. Error bars denoting SE are shown where they exceed the symbol size.

Current Fluctuation Analysis

The whole-cell recordings in DFV media were performed as described above before and after application of UTP in the bath. The cells were maintained at 0 mV holding potential and currents were recorded by applying 700-ms voltage steps to −50- and −100-mV test potentials every 5 s. The current records at each test potential were sampled at 5 kHz and filtered at 1 kHz. The mean current and variance at each test potential were calculated from 200-ms segments of the digitized current using a software written on the basis of Microsoft Excel. The background noise and leak current at every potential were subtracted from mean current and variance.

The stationary noise analysis was performed as described in (Jackson and Strange, 1995; Prakriya and Lewis, 2002) with the following assumptions: (a) the I_{CRAC} channels in the membrane are identical and independent; (b) the channels have two conductance states, open and closed; and (c) the single-channel conductance of channels in the membrane stays constant during current activation. With these assumptions, the current variance σ^2 is related to the single-channel properties as

$$\sigma^2 = I \cdot i - I^2/N + \sigma_o^2, \quad (2)$$

where σ^2 is the current variance, σ_o^2 is the variance of background noise, i is the single-channel current, N is a number of active channels in the membrane, and I is a whole cell current:

$$I = N \cdot i \cdot Po, \quad (3)$$

where Po is the single channel open probability.

Combination of Eqs. 2 and 3 leads to:

$$\sigma^2 - \sigma_o^2 = i \cdot I \cdot (1 - Po). \quad (4)$$

In general case the Eq. 4 (and the equivalent Eq. 2) is parabolic. However, the Eq. 4 adapts linear form if open channel probability is low:

$$\sigma^2 - \sigma_o^2 \cong i \cdot I, \text{ if } Po \ll 1. \quad (5)$$

Solutions

For whole-cell experiments, pipette solution contained (in mM) 145 NMDG aspartate, 10 Cs-EGTA (or 12 mM Cs-BAPTA), 10 Cs-HEPES, pH 7.3, 1.5 $MgCl_2$, and either 4.5 $CaCl_2$ (pCa 7.0) or no $CaCl_2$ added (pCa > 9). 10 μM $InsP_3$ was included in the pCa 7.0 pipette solution as indicated. Extracellular solution contained (in mM) 140 NMDG aspartate, 10 $BaCl_2$, 10 Cs-HEPES, pH 7.3. The divalent-free (DVF) solution contained (in mM) 135 Na methanesulfonate, 5 NaCl, 10 HEDTA, 0.5 EGTA, and 10 HEPES pH 7.3. For single-channel experiments, the pipette solution contained (in mM): 105 $BaCl_2$ or 140 NaCl as indicated and 10 Tris-HCl (pH 7.3). In inside-out experiments the intracellular solution contained (in mM): 140 K glutamate, 5 NaCl, 1 $MgCl_2$, 10 K-HEPES pH 7.4, 2 EGTA and 1.13 $CaCl_2$ (pCa 7.0), with or without $InsP_3$ as indicated. In cell-attached experiments, the bath solution contained (in mM): 140 KCl, 5 NaCl, 10 K-HEPES, 1 $MgCl_2$, and 2 $CaCl_2$. In outside-out experiments the same solutions were used as in whole-cell experiments. The drugs and recombinant proteins were applied to the patches by bath perfusion. The time required for a complete change of solution around the patch was less than 1 s.

Expression and Purification of Recombinant CBD-InsP$_3$R1N Proteins

CBD-$InsP_3$R1N and CBD-$InsP_3$R1N-K508R proteins were expressed in 0.5 liter of LB media for 14 h at 30°C in protease-deficient BL21 *E. coli* strain by 1 mM IPTG induction according to manufacturer's (Amersham Pharmacia Biotech) protocols. Cells were cooled on ice, collected by 20 min centrifugation at 4,500 rpm (Beckman JLA-10.5), and resuspended in 30 ml of wash buffer (20 mM TrisCl pH 8.0, 40 mM EDTA) with addition of 0.2 mg/ml lysozyme and protease inhibitors (1 mg/ml leupeptine, 200 μg/ml aprotinin, 1 mM PMSF). Cells were disrupted by repetitive 60 s sonication bursts on

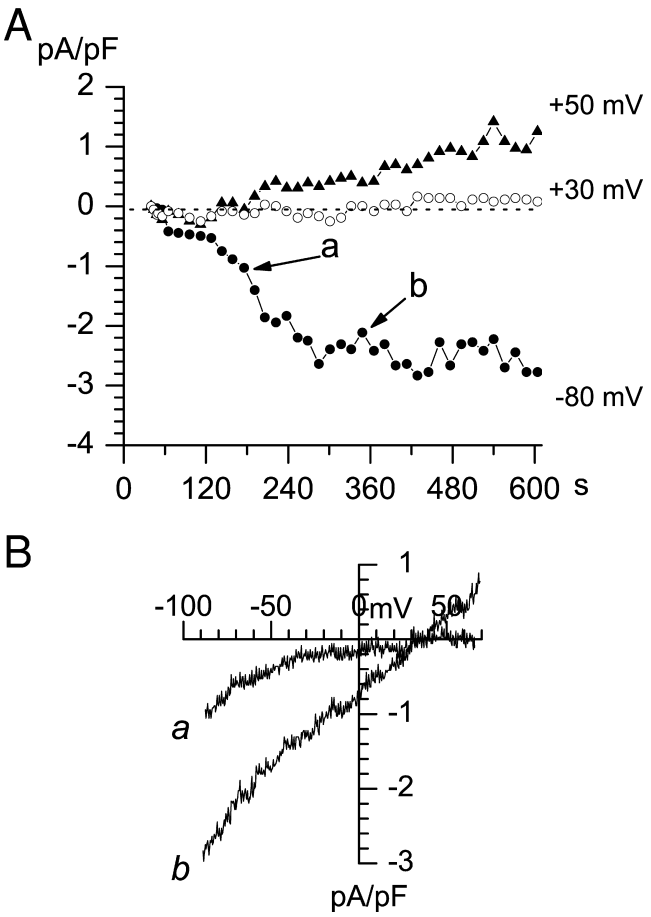

FIGURE 1. Activation of I_{CRAC} and I_{SOC} currents in A431 cells by intracellular store-depletion. Whole-cell recordings were performed at 0-mV holding potential using ramp protocol (test potentials from −100 to 70 mV; duration of the ramp, 200 ms; interramp interval is 10 s). Pipette solution contained (in mM) 10 Cs-HEPES pH 7.3, 145 NMDG aspartate, 10 Cs-EGTA (pCa > 9.0), 1.5 $MgCl_2$. Extracellular solution contained (in mM) 10 Cs-HEPES pH 7.3, 140 NMDG aspartate, 10 $BaCl_2$. (A) The amplitudes of peak currents recorded at each ramp at −80 mV (filled circles), 30 mV (open circles) and 50 mV (filled triangles) test potentials are plotted as a function of time after break-in. (B) Current-voltage relationships recorded at 159 s (curve a) and 275 s (curve b). Data from the same experiment are shown in A and B. Ramps corresponding to curves a and b in B are indicated by arrows in A. The data are representative of 19 experiments.

ice (Branson Ultrasonics). After centrifugation (4,500 *g* for 30 min; Beckman J-20 rotor) the pellet was twice washed with TED buffer (10 mM TrisCl pH 8.0, 1 mM EDTA, 1 mM DTT) and solubilized in 5 ml denaturing buffer (10 mM TrisCl pH 8.0, 8 M urea) for 3 h at RT. 5 ml of denatured protein was added to 250 ml of refolding buffer (50 mM TrisCl pH 8.0, 2 mM EDTA, 1.25 M NaCl, 0.5 M L-arginine) and incubated with stirring overnight in cold room. The resulting soluble fraction was concentrated to 5 ml on Amicon YM50 filters under nitrogen pressure and dialyzed against PBS.

[^{3}H]InsP3 Binding Assay

Specific [^{3}H]InsP3 binding was performed with minor modifications of a procedure described previously (Glouchankova et al., 2000). Briefly, 10–20 μg of purified CBD-InsP_3R1N protein was incubated on ice with 10 nM [^{3}H]InsP_3 (Amersham Pharmacia Biotech) in the binding buffer (50 mM Tris-HCl, pH 8.3, 1 mM EDTA, 1 mM DTT, 100 mM NaCl) and precipitated with 12.5% PEG and 1.2 mg/ml γ-globulin at 14,000 *g*. Precipitates were quickly washed with the binding buffer, dissolved in Soluene (Packard Instrument Co.) and their [^{3}H] content was determined by liquid scintillation counting. Nonspecific counts, determined in the presence of 25 μM nonlabeled InsP_3, were subtracted from the total to yield specific binding.

Chemicals

HEPES, NMDG, and Na-methanesulfonate were from Sigma-Aldrich; EGTA and HEDTA were from Fluka Chemie AG; and UTP and InsP_3 were from Calbiochem.

RESULTS

I_{CRAC} and I_{SOC} Divalent Whole-cell Currents in A431 Cells

To investigate store depletion–activated divalent cation influx pathways in A431 cells, we performed a series of whole-cell current recordings using 10 mM Ba^{2+} as a current carrier. To stimulate store-depletion–activated

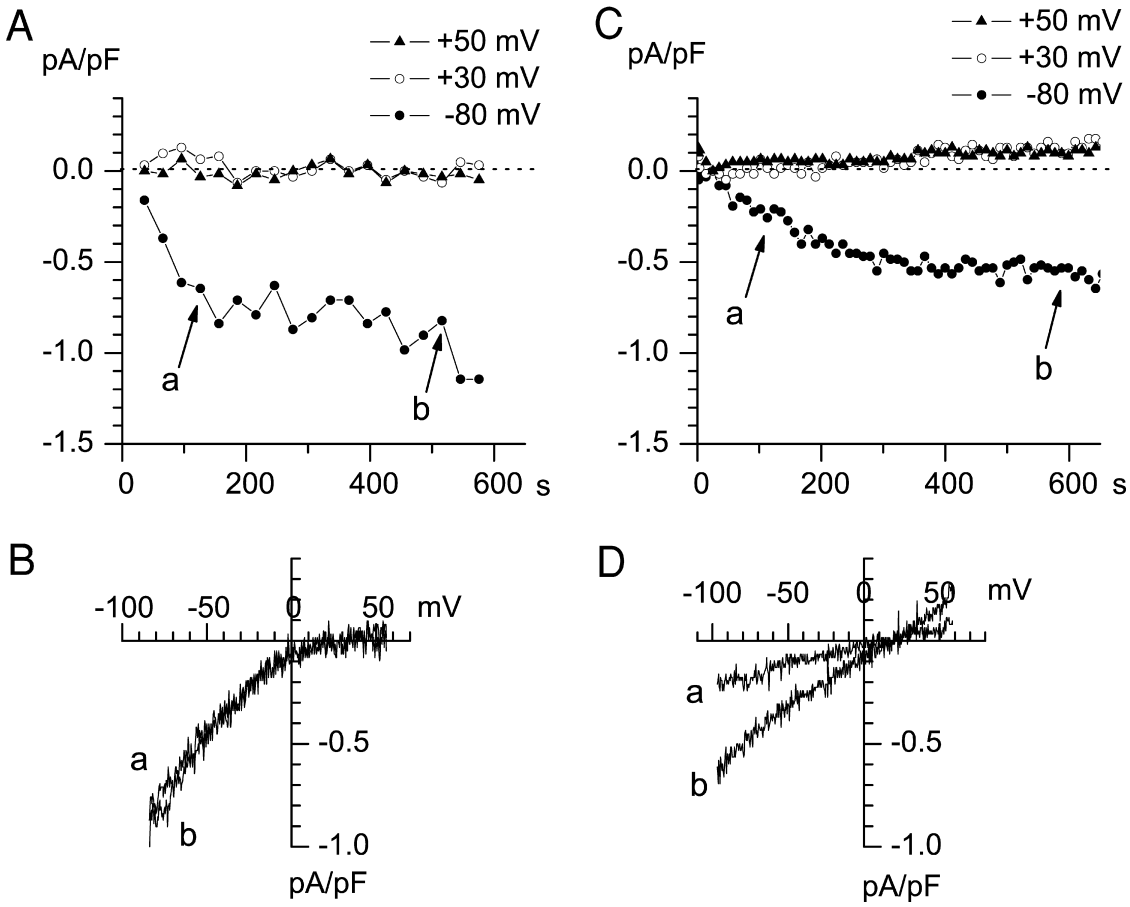

FIGURE 2. "I_{CRAC}-only" and "I_{SOC}-only" currents are activated by intracellular store-depletion. (A) Whole-cell recordings were performed as on Fig. 1 with the inter-ramp interval equal to 30 s. Pipette solution is the same as in Fig. 1 with addition of 4.5 $CaCl_2$ (pCa 7.0) and 10 μM InsP_3. Extracellular solution is the same as in Fig. 1. The amplitudes of the peak currents recorded at each ramp at −80 mV (filled circles), 30 mV (open circles), and 50 mV (filled triangles) test potentials are plotted as a function of time after break-in. (B) Current-voltage relationship recorded at 156 s (curve a) and 486 s (curve b). Ramps corresponding to curves a and b in B are indicated by arrows in A. The data are representative of 5 experiments. (C) Whole-cell recordings were performed as in Fig. 1 with the interramp interval equal to 10 s. The pipette and extracellular solutions are the same as on Fig. 2 A. The amplitudes of peak currents recorded at each ramp at −80 mV (filled circles), 30 mV (open circles), and 50 mV (filled triangles) test potentials are plotted as a function of time after break-in. (D) Current-voltage relationship recorded at 100 s (curve a) and 600 s (curve b) of the experiment. Ramps corresponding to curves a and b in D are indicated by arrows in C. The data are representative of seven experiments.

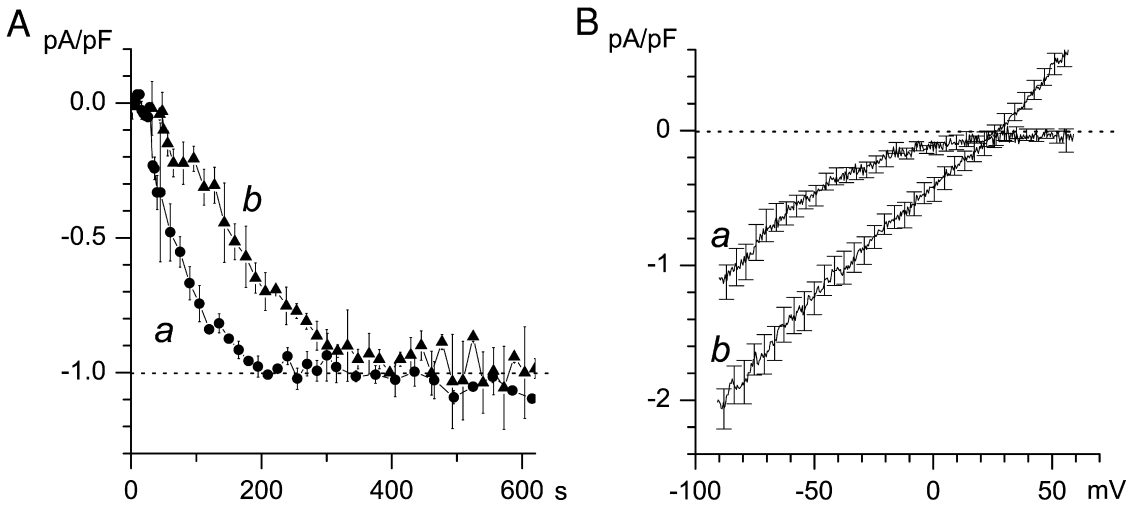

FIGURE 3. Time-course of current activation and current-voltage relationship of I_{CRAC} and I_{SOC} currents. (A) The average I_{CRAC} (filled circles, $n = 4$, curve a) and I_{SOC} (filled triangles, $n = 6$, curve b) currents are shown as a function of the time after break-in. The amplitude of the currents measured at −80 mV test potential in each experiment was normalized to the size of the currents recorded in the same experiment at 210 s for I_{CRAC} and at 400 s for I_{SOC}. (B) The average current-voltage relationship measured in cells exhibiting only I_{CRAC} currents ($n = 4$, curve a) and only I_{SOC} current ($n = 6$, curve b). To generate curve a, the current voltage-relationships were determined as shown on Fig. 2, A and B, when I_{CRAC} channels were fully activated (at least 150–200 s after break-in). To generate curve b, the current voltage-relationships were determined as shown on Fig. 2, C and D, when I_{SOC} channels were fully activated (at least 340 s after break-in). Data from the same experiments were used to generate A and B.

currents, the pipette solution contained 10 mM EGTA or 12 mM BAPTA and 1.5 mM Mg^{2+} (pCa > 9.0). The A431 cells in these experiments were maintained at 0-mV holding potential and currents were recorded using 170-ms ramps from −100 to 70 mV. The inter-ramp interval was in the range from 4 to 30 s. The amplitudes of divalent currents recorded in a representative experiment at −80-, 30-, and 50-mV test potentials are plotted as a function of time on Fig. 1 A (time = 0 at the moment of break-in). The complete current-voltage curves measured at 159 s after break-in (curve a) and 275 s after break-in (curve b) in the same experiment are shown on Fig. 1 B. It is apparent that the current-voltage curves change not only in amplitude but also in shape. The curve a (measured at 159 s) displays strong inward rectification, with no detectable outward current with test potentials as positive as 70 mV. In contrast, the curve b (measured at 275 s) is practically linear and shows significant outward current at test potentials more positive than 30 mV. Curve a (Fig. 1 B) has the shape expected for a highly Ca^{2+}–selective I_{CRAC} current described in Jurkat and RBL cells (Hoth and Penner, 1992; Zweifach and Lewis, 1993; Premack et al., 1994). The shape of curve b (Fig. 1 B) corresponds to a less Ca^{2+}–selective current.

Two alternatives could account for the observed results. The first is that A431 cells express two types of Ca^{2+} influx channels: highly Ca^{2+}–selective I_{CRAC} and less Ca^{2+}–selective store-operated channels (I_{SOC}). The second possibility is that I_{CRAC} channels activated by store depletion became less Ca^{2+} selective in the course of an experiment. Our data indicate that the coexistence of two different store-operated Ca^{2+} channel types in A431 cells is a more likely possibility. Indeed, in some cells (5/36 experiments, 14%) only highly Ca^{2+}-selective I_{CRAC} channels (Fig. 2, A and B) were observed. To facilitate Ca^{2+} store depletion, 10 μM $InsP_3$ was included in the pipette solution in addition to 10 mM EGTA and 4.5 mM $CaCl_2$ (pCa = 7.0) in the experiment shown on Fig. 2, A and B. In other cells (7/36 experiments, 19%) only moderately selective I_{SOC} currents were observed using the same pipette solution (Fig. 2, C and D). The combination of I_{CRAC} and I_{SOC} currents (Fig. 1) was observed in 19/36 experiments (53%). We could not identify the reasons for variability in I_{CRAC} and I_{SOC} current expression in A431 cells. Nevertheless, we reasoned that the existence of "I_{CRAC} only" (Fig. 2, A and B) and "I_{SOC} only" (Fig. 2, C and D) A431 cells argues against the possibility of I_{CRAC} to I_{SOC} interconversion during our recordings.

Both types of channels were activated by store depletion in our experiments, but with the different time course. Fig. 3 A illustrates an average time-course of I_{CRAC} (filled circles, $n = 4$) and I_{SOC} (filled triangles, $n = 6$) currents activation. It is apparent that I_{CRAC} current reaches maximum value within 200 s after break-in (Fig. 3 A, curve a), whereas I_{SOC} requires at least 300 s to reach its maximum value (Fig. 3 A, curve b). To further compare I_{CRAC} and I_{SOC} divalent currents in A431 cells, we calculated average current-voltage relation-

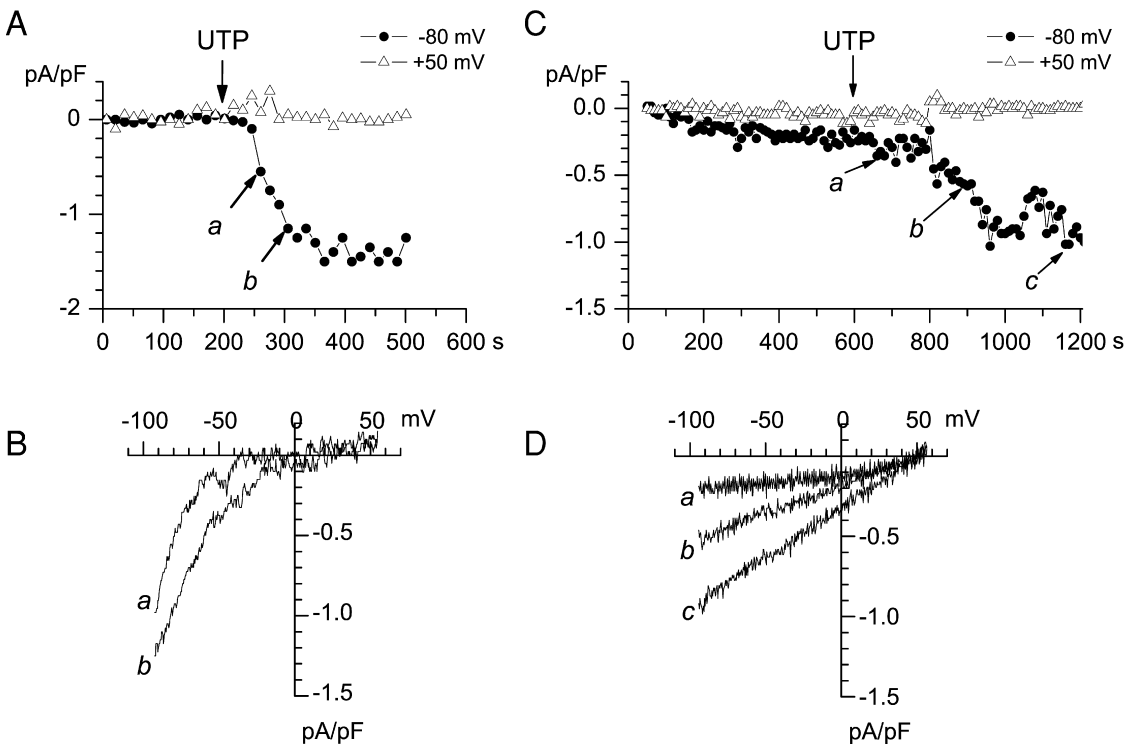

FIGURE 4. Activation of I_{CRAC} and I_{SOC} currents by extracellular UTP. Whole-cell recordings were performed with the pipette and extracellular solutions as in Fig. 2 without addition of $InsP_3$. (A) The amplitudes of peak currents recorded at each ramp at −80 mV (filled circles) and 50 mV (open triangles) test potentials are plotted as a function of time after break-in. 100 μM UTP was applied to the cells at 208 s (arrow). (B) Current-voltage relationships recorded at 231 s (curve a) and 300 s (curve b) of the experiment. Ramps corresponding to curves a and b in B are indicated by the arrows in A. (C) The amplitudes of peak currents recorded at each ramp at −80 mV (filled circles) and 50 mV (open triangles) test potentials are plotted as a function of time after break-in. 100 μM UTP was applied to the cells at 630 s (arrow). (D) The current-voltage relationships recorded at 650 s (curve a), 850 s (curve b), and 1140 s (curve c) of the experiment. Ramps corresponding to curves a–c in D are indicated by the arrows in C.

ships measured in cells containing only I_{CRAC} (Fig. 3 B, curve a, $n = 4$) or I_{SOC} (Fig. 3 B, curve b, $n = 6$) currents. To generate curve a, the current voltage-relationship was determined when I_{CRAC} channels were fully activated (Fig. 3 A, curve a). To generate curve b, I_{SOC} currents were measured at least 340 s after break-in (Fig. 3 A, curve b). On average, the amplitude of I_{CRAC} currents at −80 mV was equal to −0.96 ± 0.02 pA/pF ($n = 4$), and the amplitude of I_{SOC} currents at −80 mV was equal to −2.1 ± 0.16 pA/pF ($n = 6$). Thus, an average I_{SOC} current is twice the size of an average I_{CRAC} current. The reversal potential of I_{CRAC} currents could not be measured as we could not detect any significant outward current via I_{CRAC} channels at test potentials as positive as 60 mV in our recording conditions (Fig. 3 B, curve a). For I_{SOC} currents an average reversal potential (E_{rev}) was equal to 30 ± 3 mV ($n = 6$) (Fig. 3 B, curve b). After correction for liquid junction potential we calculated P_{Ba}/P_{Cs} selectivity ratio of I_{SOC} currents equal to 14.5 using GHK equation (Hille, 2001) as described in MATERIALS AND METHODS. Thus, divalent selectivity of I_{SOC} channels in A431 cells is similar to the divalent selectivity of I_{SOC} channels described in other nonexcitable cells (Berridge, 1995; Parekh and Penner, 1997; Nilius and Droogmans, 2001; Putney et al., 2001; Venkatachalam et al., 2002).

I_{CRAC} and I_{SOC} currents were observed in most (31/36) of the whole-cell recording experiments (86%). In a small fraction of cells (5/36, 14%), currents with very different properties were observed (unpublished data). In these cells, inward currents at −80-mV test potentials reached 10–20 pA/pF, 2–5-fold larger than typical I_{CRAC} or I_{SOC} currents (Fig. 3 B). At positive test potentials these cells displayed outward rectification leading to even larger currents at positive potentials (up to 30 pA/pF), in striking contrast with I_{CRAC} or I_{SOC} (Fig. 3 B). The reversal potential for these currents was close to 30 mV, similar to I_{SOC} currents (Fig. 3 B). Based on the large size of inward currents, moderate selectivity for divalent cations and characteristic outward rectification, we reasoned that the currents observed in these experiments correspond to I_{MagNuM} currents in A431 cells (Clapham, 2002; Hermosura et al., 2002; Kozak et al., 2002; Prakriya and Lewis, 2002). Detailed character-

ization of I_{MagNuM} currents in A431 cells was precluded by their rare occurrence in our experiments, and in the remainder of this paper we focus on the analysis of more prevalent I_{CRAC} and I_{SOC} currents.

Activation of I_{CRAC} and I_{SOC} Currents by Extracellular UTP

In experiments shown on Figs. 1–2 I_{CRAC} and I_{SOC} currents were activated by depletion of intracellular Ca^{2+} stores. This was achieved by buffering cytosolic Ca^{2+} to pCa > 9.0 with 12 mM BAPTA or 10 mM EGTA (Fig. 1) or by addition of 10 μM $InsP_3$ to cytosolic solution buffered to pCa = 7.0 (Fig. 2). In physiological situations, Ca^{2+} influx in nonexcitable cells is activated in response to activation of PLC-coupled receptors. Therefore, in the next series of experiments we used whole-cell recordings in A431 cells to measure Ba^{2+} currents activated by application of extracellular UTP. The intracellular Ca^{2+} concentration in these experiments was clamped to pCa 7.0 as in the experiments shown on Fig. 2, but no $InsP_3$ was added. In these conditions passive store depletion is slow and I_{CRAC} and I_{SOC} currents were not activated within the first 200 s after break-in (Fig. 4 A) and within 600 s (Fig. 4 C). However, we found that 100 μM extracellular UTP efficiently activated both I_{CRAC} and I_{SOC} currents in A431 cells (Fig. 4). Similar to experiments with store-depletion (Figs. 1 and 2), "I_{CRAC}-only" (Fig. 4, A and B) and "I_{SOC}-only" (Fig. 4, C and D) currents were induced in some A431 cells in response to extracellular UTP. The current-voltage relationship of UTP-activated currents (Fig. 4, B and D) was identical to currents activated by Ca^{2+} store depletion (Fig. 3 B). Thus, we concluded that both I_{CRAC} and I_{SOC} currents could be activated in A431 cells by Ca^{2+} store depletion or in response to activation of PLC-coupled receptors.

I_{CRAC} and I_{SOC} Monovalent Whole-cell Currents in A431 Cells

To further characterize I_{CRAC} and I_{SOC} currents in A431 cells, we performed a series of whole-cell recording experiments in DVF media containing 140 mM Na^+. In the absence of divalent cations, Na^+ and other monovalent cations carry a substantial current through voltage-gated Ca^{2+} channels (Almers et al., 1984; Hess and Tsien, 1984) and I_{CRAC} (Hoth and Penner, 1993; Hermosura et al., 2002; Prakriya and Lewis, 2002). In most of the experiments performed in DVF media, large monovalent inward and outward currents were observed (Fig. 5 A). Similar to experiments with Ba^{2+} as a current carrier (Fig. 1), the shape of the current-voltage relationship recorded in DVF media was changing in a course of the experiments. Within the first 10 s after addition of DVF solution the current-voltage relationship displayed inward rectification, and outward currents were absent with test potentials as positive as 80 mV (Fig. 5 B, curve a). At later times, the current-voltage relationship became more linear, with a reversal potential at 0 mV and large outward currents (Fig. 5 B, curve b). The amplitude of Na^+-currents continued to rise during first 10 min of recordings (Fig. 5 A). Thus, similar to recordings with Ba^{2+}, recordings in DVF media revealed two types of channels in A431 cells activated in our recording conditions. The inwardly rectifying monovalent current observed in our experiments in DVF media (Fig. 5 B, curve a) is similar to Na-I_{CRAC} current recorded in Jurkat and RBL cells (Hoth and Penner, 1993; Hermosura et al., 2002; Prakriya and Lewis, 2002). The large nonselective current observed in our experiments in DFV media (Fig. 5 B, curve b) is likely to correspond to Na-I_{SOC} currents.

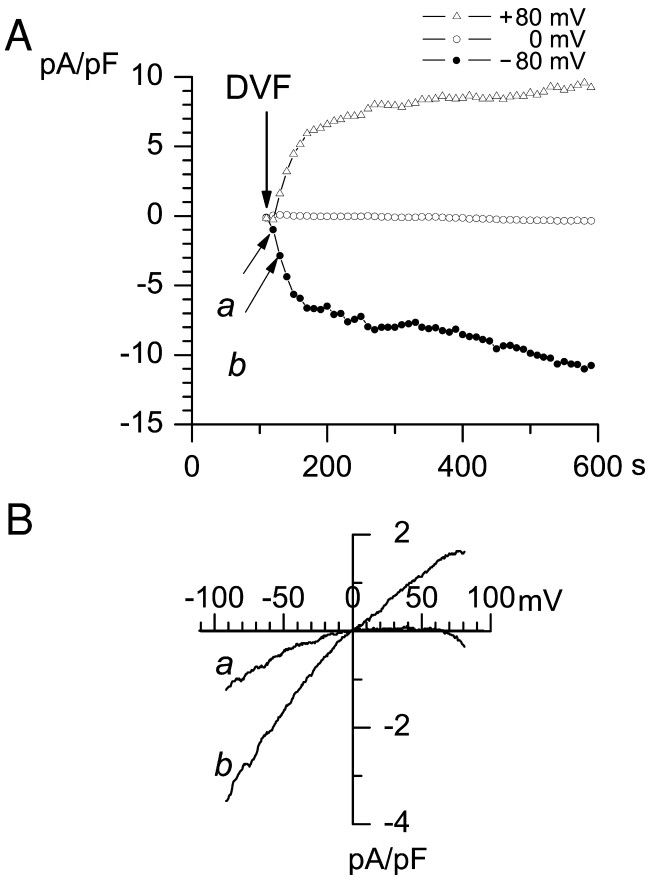

FIGURE 5. I_{CRAC} and I_{SOC} currents in DVF medium. Whole-cell recordings were performed as described in Fig. 1 with the interramp interval of 11 s. Pipette solution contained (in mM) 120 Cs-Aspartate, 10 BAPTA (pCa > 9.0), 1.5 $MgCl_2$, pH 7.3. Extracellular DVF solution contained (in mM): 135 Na-methansulfonate, 5 NaCl, 10 HEDTA, 0.5 EGTA, pH 7.3. (A) Amplitudes of peak currents recorded at each ramp at −80 mV (filled circles), 0 mV (open circles), and 80 mV (open triangles) test potentials are plotted as a function of time after break-in. Extracellular solution was replaced by DVF medium at 100 s after break-in (arrow). (B) Current-voltage relationship recorded at 120 s (curve a) and 130 s (curve b) of the experiment. Ramps corresponding to curves a and b in B are indicated by arrows in A. The data are representative of four experiments in DVF medium.

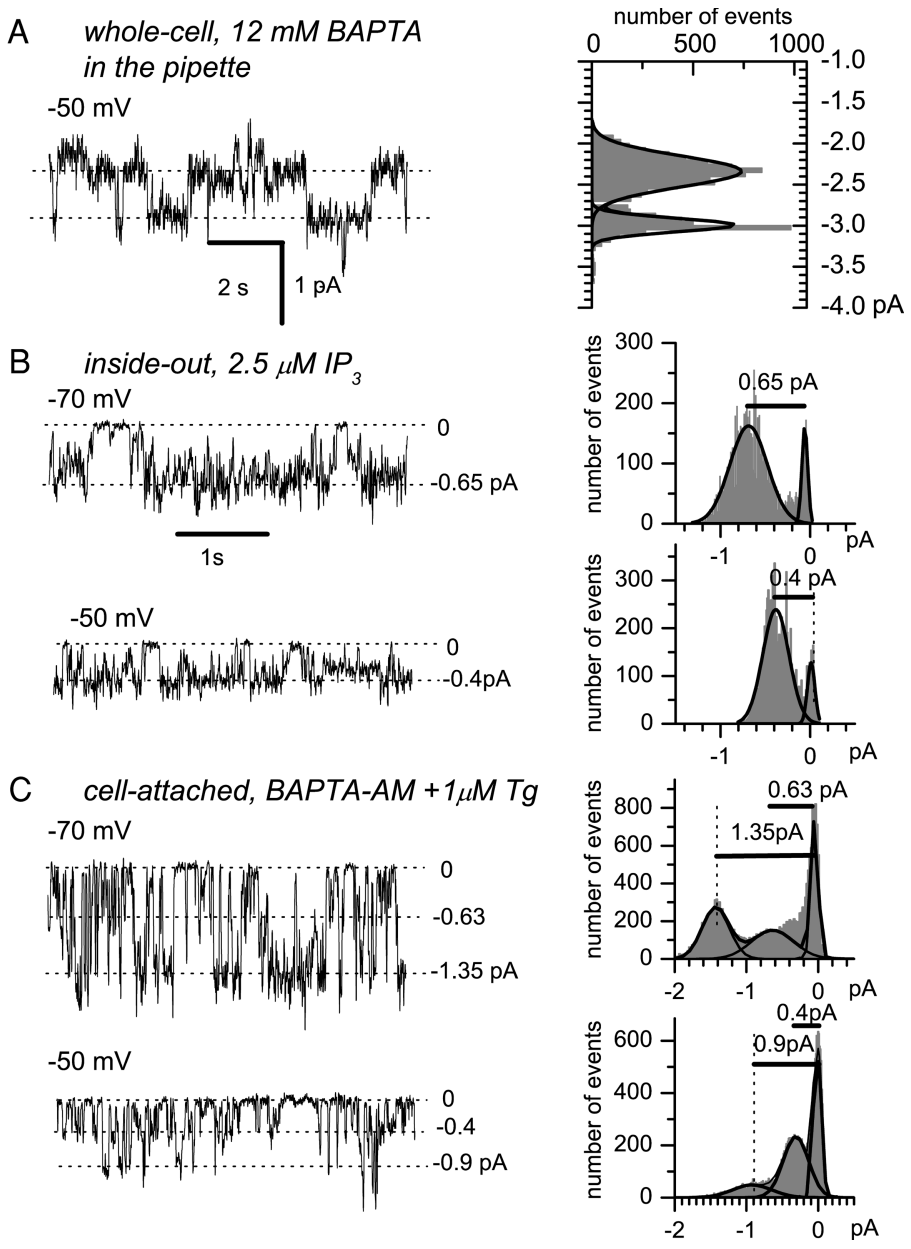

FIGURE 6. Patch-clamp recordings of single-channel activity. Single-channel activity recorded in whole-cell (A), inside-out (B), and cell-attached (C) patch-clamp mode. 140 mM Na^+ is a current carrier in all experiments (see MATERIALS AND METHODS for details). The single-channel activity was induced by: (A) store-depletion (12 mM BAPTA and 1.5 mM Mg^{2+} in the pipette, pCa > 9.0), representative of four whole-cell experiments; (B) 2.5 μM intracellular $InsP_3$, representative of 8 inside-out experiments; (C) BAPTA-AM and 100 μM Tg in cell-attached mode, representative of four cell-attached experiments. The unitary current amplitudes were measured manually or determined from all-point amplitude histograms (shown on the right).

I_{min}/I_{CRACL} Channels Support I_{SOC} Currents in A431 Cells

To gain insight into properties of channels supporting I_{CRAC} and I_{SOC} currents in A431 cells, we performed a series of single-channel recordings. In these experiments we took advantage of increased conductance of these channels in DVF media (Fig. 5). Because of different time course of I_{CRAC} and I_{SOC} activation (Fig. 3 A), we reasoned that the channels recorded within first 100 s after break-in are more likely to correspond to I_{CRAC}, and the channels recorded between 300–600 s after break-in are more likely to correspond to I_{SOC}. To measure single-channel currents in whole-cell experiments, we applied 10-s test pulses from −100 to 50 mV from the holding potential of 0 mV. In these experiments we failed to observe any channel activity within the first 100 s after break-in. However, with 12 mM BAPTA and 1.5 mM Mg^{2+} in the pipette (pCa > 9.0), we observed activity of multiple channels 200–600 s after break-in (Fig. 6 A). On average, the single-channel current through the channels was equal to 0.7 ± 0.05 pA at −70 mV test potential (Fig. 7, triangles, $n = 4$).

Channels with similar properties were recorded in excised patches after application of 2.5 μM $InsP_3$ (inside-out, Fig. 6 B, $n = 8$), and after application of 1 μM thapsigargin and 1 mM BAPTA-AM (cell-attached, Fig. 6 C, $n = 4$; see also Kaznacheyeva et al., 2001) and in outside-out configuration in response to application of extracellular UTP ($n = 4$, current records not shown). The single-channel slope conductances for channels

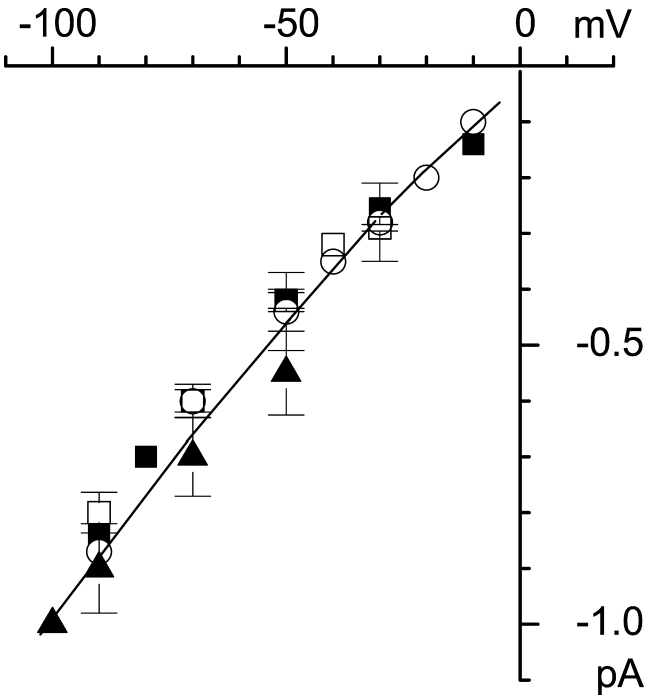

FIGURE 7. Single-channel current-voltage relationships. The mean current-voltage relationship of single channels activated by store-depletion in whole cell mode (filled triangles, $n = 4$), by 2.5 μM intracellular $InsP_3$ in inside-out mode (open circles, $n = 8$), by 100 μM Tg + BAPTA-AM in cell-attached mode (open squares, $n = 4$), or by 100 μM extracellular UTP in outside-out mode (filled squares, $n = 4$). The currents measured at several independent experiments from all-point amplitude histograms were averaged at the same test potential and shown as mean ± SEM for each recording condition. The single-channel slope conductance (line) at different potentials is 8.5–10 pS.

measured in all these experimental conditions were in the range 8.5–10 pS (Fig. 7). The properties of these channels are identical to the properties of I_{min}/I_{CRACL} channels that we described previously (Kaznacheyeva et al., 2001). Importantly, I_{min}/I_{CRACL} single-channels were observed in our whole-cell experiments from 100 s until 20 min after break-in, that is during the time period corresponding to I_{SOC} activation (Fig. 3 A).

We did not observe I_{min}/I_{CRACL} channel activity in whole-cell experiments within the first 100 s after break-in, that is in the time window of I_{CRAC} current development (Fig. 3 A). From these experiments we concluded that the previously described I_{min}/I_{CRACL} channels (Mozhayeva et al., 1990; Kiselyov et al., 1997, 1999b; Zubov et al., 1999; Kaznacheyeva et al., 2000, 2001) support I_{SOC} currents in A431 cells.

Current Fluctuation Analysis of Na-I_{CRAC}

As described above, we were unable to measure single-channel activity of I_{CRAC} channels using DVF media, most likely due to small conductance of these channels. Current fluctuation analysis has been used previously in studies of I_{CRAC} channels in Jurkat cells (Zweifach and Lewis, 1993; Prakriya and Lewis, 2002). Here we applied the stationary current fluctuation analysis method (see MATERIALS AND METHODS) to estimate the size of single-channel sodium currents via I_{CRAC} channels activated by application of 100 μM UTP to A431 cells (Fig. 8 A). To perform fluctuation analysis, we selected experiments in DVF media with "I_{CRAC}-only" cells as determined by the inward rectification shape of current-voltage relationship (Fig. 8, A and B). The intracellular Ca^{2+} concentration in these experiments was clamped to pCa 7.0 by 10 mM EGTA as in the experiments shown on Fig. 2. The mean macroscopic current (I) and corresponding variance (σ^2) were measured at holding potential of 0 mV and at −50 and −100 mV test potentials as described in MATERIALS AND METHODS. Application of UTP activated I_{CRAC} (Fig. 8 A) and caused a significant increase in the noise of the current recorded at −100 mV test potential (Fig. 8 C).

To determine the single-channel conductance of Na-I_{CRAC}, we measured variance of the UTP-activated DVF current at 0, −50, and −100 mV membrane potentials. Plots of the current variance against mean current amplitude at 0, −50, and −100 mV could well be fitted by the straight lines (Fig. 8 D). Because of the observed linear relationship between σ^2 and I we used linear approximation for relationship between σ^2 and I (MATERIALS AND METHODS, Eq. 5) in our calculations. The underlying assumption for linear approximation is that Na-I_{CRAC} open channel probability Po is low (Jackson and Strange, 1995; Prakriya and Lewis, 2002). According to Eq. 5, the slope of σ^2 versus I linear fit is equal to i, where i is the size of the Na-I_{CRAC} single channel current. The fit to the data yielded the slope equal to −0.09 pA at 0 mV (Fig. 8 D, bottom), −0.14 pA at −50 mV (Fig. 8 D, middle), and −0.18 pA at −100 mV (Fig. 8 D, top). Obtained measurements are consistent with the slope single-channel conductance of Na-I_{CRAC} channels in A431 cells equal to 0.9 pS (Fig. 8 E), which is 5 times greater than the chord conductance estimated for Na-I_{CRAC} currents in Jurkat cells (Prakriya and Lewis, 2002), and 10 times smaller than the single-channel conductance of Na-I_{soc} in A431 cells (Fig. 7). The reasons for differences between our estimates and the results of Prakriya and Lewis (2002) may reflect the differences in I_{CRAC} properties in A431 and Jurkat cells, or may be related to assumptions about channel open probability and gating properties inherent to the current fluctuation analysis approach.

Activation of I_{min}/I_{CRACL} Channels by $InsP_3R1N$

What mechanism is responsible for activation of I_{min}/I_{CRACL} channels in A431 cells? Our previous results suggested that I_{min}/I_{CRACL} channels may be activated via di-

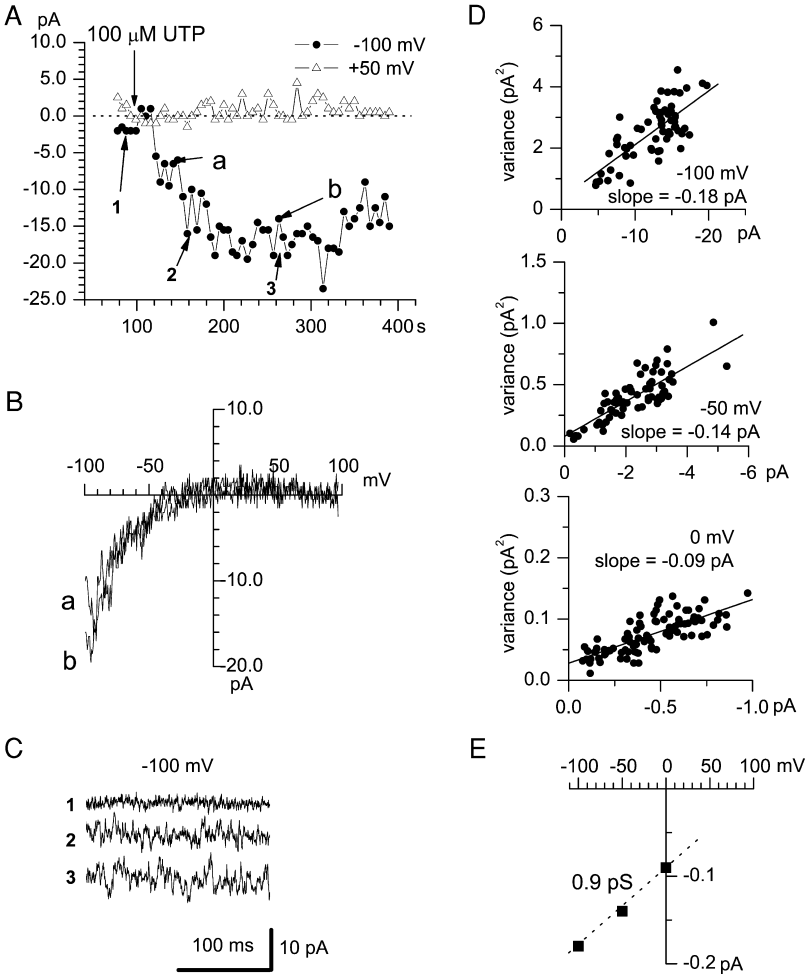

FIGURE 8. Fluctuation analysis of monovalent I_{CRAC} currents. Whole-cell recordings in DVF media were performed as described in Fig. 4. The amplitudes of peak currents recorded at each ramp at −100 mV (filled circles) and 50 mV (open triangles) test potentials are plotted as a function of the time after break-in. 100 μM UTP was applied to the cells at 105 s (arrow). (B) Current-voltage relationships recorded at 158 s (curve a) and 278 s (curve b) of the experiment. Ramps corresponding to curves a and b in B are indicated by the arrows in A. The shapes of curves a and b are indicative of "I_{CRAC}-only" cell. (C) Examples of 200-ms segments of currents recorded at −100 mV membrane potential before (1) and after (2 and 3) UTP application as indicated by the arrows in A. (D) Mean-variance analysis of Na-I_{CRAC} currents. The plots show the mean value and variance of 200-ms current sweeps collected during development of agonist-induced Na^+ current in DVF solution. The data points are fit by the straight lines with a slope of −0.18 pA (−100 mV), −0.14 pA (−50 mV), and −0.09 pA (0 mV). The data are representative of three independent experiments. (E) Current-voltage relationship of Na-I_{CRAC} single channels obtained from current measurements as shown in D. The data points are fit by a line with a slope of 0.9 pS.

rect conformational coupling with the $InsP_3R$ (Zubov et al., 1999) or with the $InsP_3R$–PIP_2 complex (Kaznacheyeva et al., 2000). Which domain of the $InsP_3R$ is required for I_{min}/I_{CRACL} activation? Based on its functional properties I_{min}/I_{CRACL} is likely to be encoded by a member of the TRPC family (see DISCUSSION). Activation of TRPC3 channels by the amino-terminal region of $InsP_3R1$ ($InsP_3R1N$) has been reported (Kiselyov et al., 1999a). Can $InsP_3R1N$ gate I_{min}/I_{CRACL}? To answer this question, we expressed the $InsP_3R1N$ fragment (aa 2–604) in bacteria as CBD-fusion protein (see MATERIALS AND METHODS). In addition, we also generated and expressed a CBD-$InsP_3R1N$-K508R mutant, which has been reported to lack specific $InsP_3$ binding activity (Yoshikawa et al., 1996).

When expressed in *E. coli* BL21 cells, both CBD-$InsP_3R1N$ and CBD-$InsP_3R1N$-K508R proteins were concentrated in inclusion bodies. In our experiments we purified the inclusion body fraction from bacteria, dissolved them in 8 M urea and refolded denatured proteins by rapid dilution. Refolded proteins were concentrated, dialyzed against PBS and used in functional experiments. Similar yields of CBD-$InsP_3R1N$ and CBD-$InsP_3R1N$-K508R proteins were obtained in this purification scheme, but only CBD-$InsP_3R1N$ protein displayed specific [^{3}H]-$InsP_3$ binding activity (unpublished data). Thus, in agreement with the report published previously (Yoshikawa et al., 1996) and with the recently reported structure of the $InsP_3R1$ ligand-binding core (Bosanac et al., 2002), the K508 residue plays a critical role in $InsP_3$ binding.

To test functional effects of $InsP_3R1N$, we applied the CBD-$InsP_3R1N$ protein to inside-out patches excised from A431 cells using 105 mM Ba^{2+} in the pipette as a current carrier. As described previously (Mozhayeva et al., 1990; Kiselyov et al., 1997, 1999b; Zubov et al., 1999; Kaznacheyeva et al., 2000, 2001), a low activity of I_{min}/I_{CRACL} channels was observed in excised patches in the presence of 2.5 μM of $InsP_3$ (Figs. 9 A and 10 B). Addition of CBD-$InsP_3R1N$ protein to the cytosolic surface of the patch resulted in rapid facilitation of I_{min}/I_{CRACL} channel activity (Figs. 9 A and 10 B). These channels displayed 1.5 pS conductance in 105 mM Ba^{2+} (Fig. 9 C), as described previously for I_{min}/I_{CRACL} (Mozhayeva et al., 1990; Kiselyov et al., 1997, 1999b; Zubov et al., 1999; Kaznacheyeva et al., 2000, 2001).

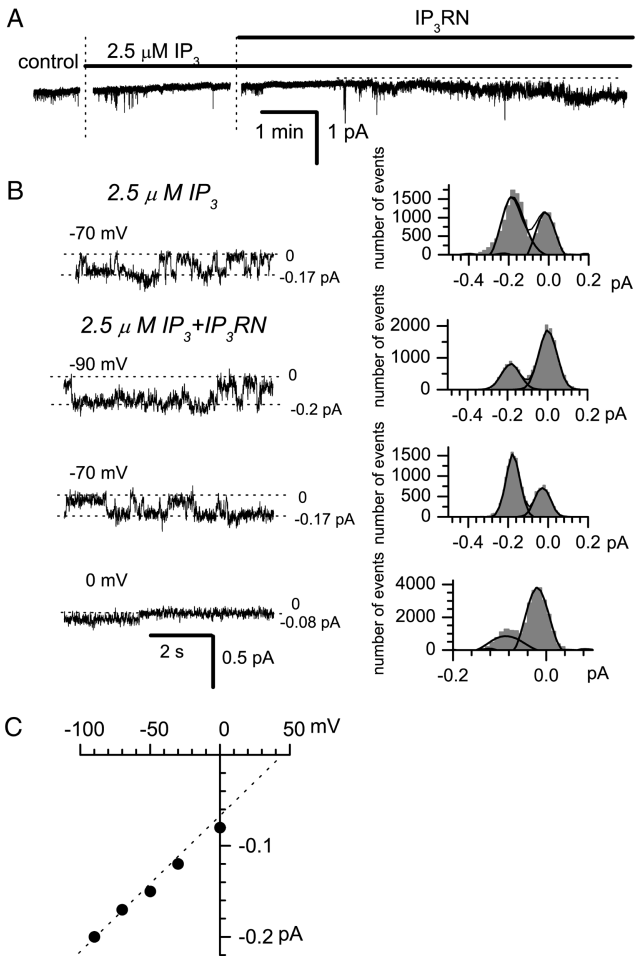

FIGURE 9. $InsP_3R1N$ activates I_{min}/I_{CRACL} in inside-out patches. (A) Current traces in an inside-out patch recorded after application of $InsP_3$ and CBD-$InsP_3R1N$ at −70 mV holding potential. (B) The current induced by $InsP_3$ and CBD-$InsP_3R1N$ was recorded at the membrane potentials as indicated. Currents amplitudes were measured from all-point amplitude histograms (shown on the right). (C) The current-voltage relationship of I_{min}/I_{CRACL} channels activated by $InsP_3$ and CBD-$InsP_3R1N$. The single-channel slope conductance (line) is 1.5 pS. Data are representative of 13 experiments.

Can $InsP_3R1N$ activate I_{min}/I_{CRACL} channels independently from $InsP_3$? When CBD-$InsP_3R1N$ was added to excised patches in the absence of $InsP_3$, no channel activity was observed (Fig. 10 A). However, addition of $InsP_3$ to the same patch resulted in an immediate activation of I_{min}/I_{CRACL} channels (Fig. 10 A). Thus, $InsP_3$ is required for $InsP_3R1N$ activation of I_{min}/I_{CRACL} channels. Is $InsP_3$ binding to $InsP_3R1N$ important for the observed functional effects? When CBD-$InsP_3R1N$-K508R protein was added to inside-out patches in the presence of 2.5 μM of $InsP_3$, no channel activity was observed (Fig. 10 B). In contrast, addition of CBD-$InsP_3R1N$ to the same patch induced I_{min}/I_{CRACL} activity (Fig. 10 B). These data suggest that the $InsP_3$-liganded form of $InsP_3R1N$ is a true activator of I_{min}/I_{CRACL} channels.

DISCUSSION

Store-operated Ca^{2+} influx pathways in A431 cells were analyzed in this paper by whole-cell and single-channel recordings. We discovered that I_{CRAC} and I_{SOC} currents are present in A431 cells. The main functional properties of I_{CRAC} and I_{SOC} (I_{min}/I_{CRACL}) channels in A431 and other nonexcitable cells are briefly summarized in Table I. Implications of our findings are discussed below.

I_{min}/I_{CRACL} and I_{CRAC}

In the previous patch-clamp studies we described store-operated and $InsP_3$-activated I_{min}/I_{CRACL} channels in A431 cells (Mozhayeva et al., 1990; Kiselyov et al., 1997, 1999b; Zubov et al., 1999; Kaznacheyeva et al., 2000, 2001). Some of the properties of I_{min}/I_{CRACL} channels, such as sensitivity to store-depletion, small conductance for divalent and monovalent cations, and sensitivity to block by SKF95365, indicated that I_{min}/I_{CRACL} channels may correspond to I_{CRAC} channels in A431 cells. However, a number of differences between I_{min}/I_{CRACL} and I_{CRAC} currents were uncovered in the present study. The main differences between I_{min}/I_{CRACL} channels and I_{CRAC} channels are (Table I): (a) I_{min}/I_{CRACL} conductance for divalent cations is 1–1.5 pS, for I_{CRAC} it is estimated at 10–25 fS; (b) I_{min}/I_{CRACL} conductance for sodium is 8.5–10 pS, for I_{CRAC} it is estimated at 0.2–0.9 pS; (c) I_{min}/I_{CRACL} channels are moderately selective for divalent cations (P_{Ba}/P_{Cs} = 14.5), I_{CRAC} channels are highly selective for divalent cations ($P_D/P_M > 1{,}000$); (d) I_{min}/I_{CRACL} channels display linear current-voltage relationship, I_{CRAC} currents display inward rectification; and (e) I_{min}/I_{CRACL} currents require at least 300 s after initiation of Ca^{2+} store depletion for complete activation, I_{CRAC} currents activate within 100–200 s. Thus, we concluded that I_{min}/I_{CRACL} channels and I_{CRAC} channels are different entities. In support of this conclusion, I_{CRAC}-only cells were found in 5 of 36 whole-cell experiments (14%) and I_{min}/I_{CRACL}-only currents were found in 7 of 36 experiments (19%). In 19 of 36 experiments (53%), both types of currents were present in the same cell. The different rates of I_{CRAC} and I_{min}/I_{CRACL} activation in response to store-depletion (Fig. 3 A) suggest that these two Ca^{2+} entry pathways could be gated by different mechanisms. Another possibility is that both I_{CRAC} and I_{min}/I_{CRACL} are activated by a similar "conformational coupling" mechanism (see below), but coupled to different Ca^{2+} pools, so that I_{CRAC} is coupled to the pool that is depleted rapidly, and I_{min}/I_{CRACL} is

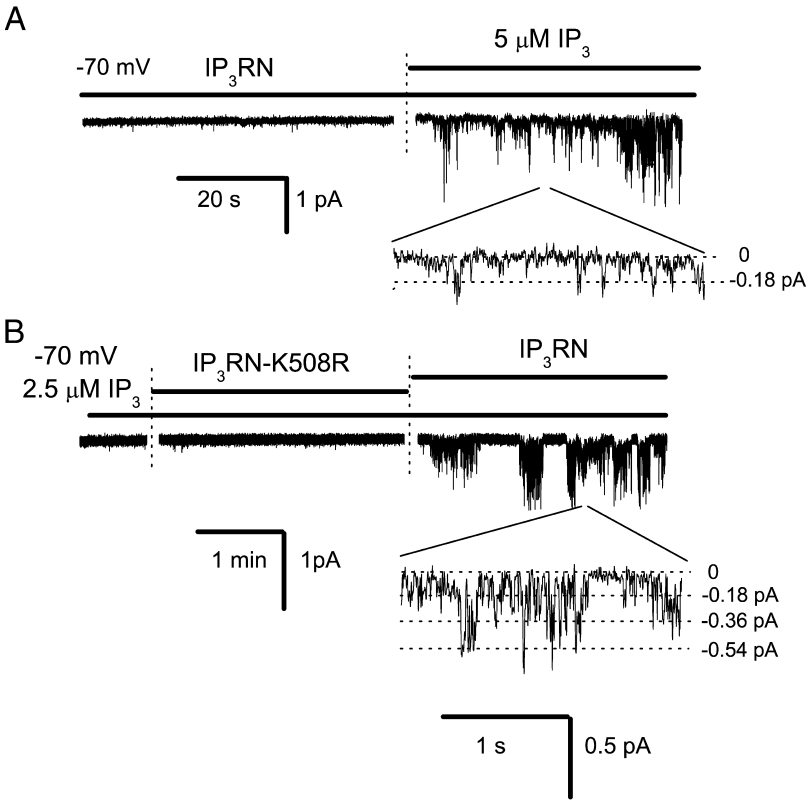

FIGURE 10. $InsP_3$ binding to $InsP_3R1N$ is required for I_{min}/I_{CRACL} activation. Inside-out patch clamp recordings of I_{min}/I_{CRACL} channel activity were performed as described in Fig. 9 at −70 mV. (A) $InsP_3$ is required for I_{min}/I_{CRACL} channel activation by CBD-$InsP_3R1N$. I_{min}/I_{CRACL} currents are shown on compressed (top) and expanded (bottom) time scales. Data are representative of eight experiments. (B) $InsP_3R1N$, but not $InsP_3R1N$-K508R, evokes I_{CRACL} activity. I_{min}/I_{CRACL} current activity in response to application of $InsP_3$, CBD-$InsP_3R1N$-K508R, and CBD-$InsP_3R1N$ to the patch is shown as indicated. I_{min}/I_{CRACL} currents are shown on compressed (top) and expanded (bottom) time scales.

coupled to the pool that is depleted more slowly. The differences in the rates of pool depletion can be related to the differences in distribution of $InsP_3R$ and Ca^{2+} pumps, as well as to localized expression of different $InsP_3R$ isoforms. Future experiments will be needed to discriminate between these possibilities.

TABLE I

Comparison of I_{CRAC} and I_{SOC} (I_{min}/I_{CRACL}) Functional Properties

Property	I_{CRAC}	ISOC (I_{min}/I_{CRACL})
Conductance		
Divalent cations	~25 fS (Zweifach and Lewis, 1993)	1.5 pS (Kaznacheyeva et al., 2001)
DVF	0.2–0.9 pS (Fig. 8 E; Prakriya and Lewis, 2002)	8.5–10 pS (Fig. 7; Kaznacheyeva et al., 2001)
Divalant current size in A431 cells	1 pA/pF (Fig. 3 B)	2 pA/pF (Fig. 3 B)
Permeability ratio		
$P_{D/M}$	>1,000 (Hoth and Penner, 1993; Zweifach and Lewis, 1993)	14.5 (Fig. 3 B)
$P_{Na/Cs}$	~10 (Hermosura et al., 2002; Prakriya and Lewis, 2002)	~1 (Fig. 5 B)
IVC		
Divalent currents	Inward rectification (Fig. 3 B; Hoth and Penner, 1993; Zweifach and Lewis, 1993)	Linear (Fig. 3 B)
DVF	Inward rectification (Fig. 5 B; Hermosura et al., 2002; Prakriya and Lewis, 2002)	Linear (Fig. 5 B)
Block by Mg^{2+}	No (Fig. 2 A)	No (Fig. 2 C)
Activation by store depletion	Yes (Fig. 1; Hoth and Penner, 1993; Zweifach and Lewis, 1993)	Yes (Figs. 1, 6 A, 6 C; Kaznacheyeva et al., 2001)
By $InsP_3$	Yes (Fig. 2 A; Hoth and Penner, 1993; Zweifach and Lewis, 1993)	Yes (Figs. 2 C and 6 B; Kaznacheyeva et al., 2001)
By PLC-linked agonists	Yes (Fig. 4 A; Hoth and Penner, 1993; Zweifach and Lewis, 1993)	Yes (Figs 4 C; Kaznacheyeva et al., 2001)
PIP_2	ND	Inhibits (Kaznacheyeva et al., 2000)
Onset of current	<100 s (Fig. 3 A; Hermosura et al., 2002; Prakriya and Lewis, 2002)	>200 s (Fig. 3 A)
Block by SKF96365	Complete block by 20 μM (Franzius et al., 1994; Prakriya and Lewis, 2002)	Complete block by 25 μM (Zubov et al., 1999)

I_{min}/I_{CRACL} and TRPC

Our results lead us to conclude that I_{min}/I_{CRACL} channels support I_{SOC} current in A431 cells. What is the molecular identity of I_{min}/I_{CRACL} channels? Recent results support the hypothesis that members of the TRPC family are essential components of I_{SOC} channels in nonexcitable cells. Indeed, genetic knockout of the TRPC4 subunit in mouse resulted in dramatic reduction of I_{SOC} currents in endothelial cells (Freichel et al., 2001). Similar results were obtained when TRPC1 was genetically deleted in chicken B cell lymphocytes (Mori et al., 2002). Thus, it is likely that I_{SOC} currents in other nonexcitable cells are also supported by the members of TRPC family. The main functional properties of I_{min}/I_{CRACL} channels are consistent with the properties of channels formed by TRPC family members when expressed in heterologous expression system (for review see Birnbaumer et al., 1996; Clapham et al., 2001; Nilius and Droogmans, 2001; Montell et al., 2002; Venkatachalam et al., 2002; Zitt et al., 2002). Future molecular studies will be required to test this hypothesis and to identify the TRPC protein that encodes I_{min}/I_{CRACL} channels in A431 cells.

I_{min}/I_{CRACL} and $InsP_3R$

What is a mechanism of I_{min}/I_{CRACL} activation? Our previous results (Zubov et al., 1999; Kaznacheyeva et al., 2000) supported the conformational coupling model of I_{min}/I_{CRACL} activation. Here we provide additional evidence in favor of the conformational coupling model. We established that the amino-terminal fragment of $InsP_3R1$ ($InsP_3R1N$) was able to activate I_{min}/I_{CRACL} in excised inside-out patches (Fig. 9) and that $InsP_3R1N$ association with $InsP_3$ is critical for I_{min}/I_{CRACL} channel activation (Fig. 10). Importantly, the $InsP_3R1N$ fragment used in our experiments (amino acids 2–604) does not contain previously identified TRPC3- and TRPC4-binding sites, which are located within 669–821 region (Boulay et al., 1999; Tang et al., 2001). Thus, it is unlikely that the direct association of $InsP_3R1N$ with a member of TRPC family can account for an ability of $InsP_3R1N$ to activate I_{min}/I_{CRACL}. Most likely, an additional adaptor protein is involved in the conformational coupling between $InsP_3R$ and I_{min}/I_{CRACL} (TRPC). One potential candidate for this role is a Homer protein (Xiao et al., 2000) that binds to the residues 48–55 of the $InsP_3R1$ amino-terminal region (Tu et al., 1998), which are present within $InsP_3R1N$ sequence. Identification of additional $InsP_3R1$ amino-terminal binding partners may provide interesting insights into $InsP_3R1$-I_{min}/I_{CRACL} conformational coupling mechanism.

The authors are grateful to Dr. Bertil Hille for comments on the paper and to V. Alexeenko for technical support.

Supported by the Russian Basic Research Foundation 01-04-48809 (E. Kaznacheyeva), 01-04-48810 (G.N. Mozhayeva), SS-2178.2003.4 (G.N. Mozhayeva), the program of "Physical-Chemical Biology" Russian Academy of Sciences (G.N. Mozhayeva), the National Institutes of Health NS38082 (I. Bezprozvanny), the Robert J. Welch Foundation (I. Bezprozvanny), and the CRDF RB1-2018 (G.N. Mozhayeva and I. Bezprozvanny).

Olaf S. Andersen served as editor.

Submitted: 10 February 2003
Revised: 22 May 2003
Accepted: 23 May 2003

REFERENCES

Almers, W., E.W. McCleskey, and P.T. Palade. 1984. A non-selective cation conductance in frog muscle membrane blocked by micromolar external calcium ions. *J. Physiol.* 353:565–583.

Barry, P.H. 1994. JPCalc, a software package for calculating liquid junction potential corrections in patch-clamp, intracellular, epithelial and bilayer measurements and for correcting junction potential measurements. *J. Neurosci. Methods.* 51:107–116.

Berridge, M.J. 1995. Capacitative calcium entry. *Biochem. J.* 312:1–11.

Birnbaumer, L., X. Zhu, M. Jiang, G. Boulay, M. Peyton, B. Vannier, D. Brown, D. Platano, H. Sadeghi, E. Stefani, and M. Birnbaumer. 1996. On the molecular basis and regulation of cellular capacitative calcium entry: roles for Trp proteins. *Proc. Natl. Acad. Sci. USA.* 93:15195–15202.

Bosanac, I., J.R. Alattia, T.K. Mal, J. Chan, S. Talarico, F.K. Tong, K.I. Tong, F. Yoshikawa, T. Furuichi, M. Iwai, et al. 2002. Structure of the inositol 1,4,5-trisphosphate receptor binding core in complex with its ligand. *Nature.* 420:696–700.

Boulay, G., D.M. Brown, N. Qin, M. Jiang, A. Dietrich, M.X. Zhu, Z. Chen, M. Birnbaumer, K. Mikoshiba, and L. Birnbaumer. 1999. Modulation of Ca^{2+} entry by polypeptides of the inositol 1,4,5-trisphosphate receptor (IP_3R) that bind transient receptor potential (TRP): evidence for roles of TRP and IP3R in store depletion-activated Ca^{2+} entry. *Proc. Natl. Acad. Sci. USA.* 96:14955–14960.

Clapham, D.E. 1996. TRP is cracked but is CRAC TRP? *Neuron.* 16: 1069–1072.

Clapham, D.E. 2002. Sorting out MIC, TRP, and CRAC ion channels. *J. Gen. Physiol.* 120:217–220.

Clapham, D.E., L.W. Runnels, and C. Strubing. 2001. The TRP ion channel family. *Nat. Rev. Neurosci.* 2:387–396.

Csutora, P., Z. Su, H.Y. Kim, A. Bugrim, K.W. Cunningham, R. Nuccitelli, J.E. Keizer, M.R. Hanley, J.E. Blalock, and R.B. Marchase. 1999. Calcium influx factor is synthesized by yeast and mammalian cells depleted of organellar calcium stores. *Proc. Natl. Acad. Sci. USA.* 96:121–126.

Estacion, M., W.G. Sinkins, and W.P. Schilling. 2001. Regulation of *Drosophila* transient receptor potential-like (TrpL) channels by phospholipase C-dependent mechanisms. *J. Physiol.* 530:1–19.

Franzius, D., M. Hoth, and R. Penner. 1994. Non-specific effects of calcium entry antagonists in mast cells. *Pflugers Arch.* 428:433–438.

Freichel, M., S.H. Suh, A. Pfeifer, U. Schweig, C. Trost, P. Weissgerber, M. Biel, S. Philipp, D. Freise, G. Droogmans, et al. 2001. Lack of an endothelial store-operated Ca^{2+} current impairs agonist- dependent vasorelaxation in $TRP4^{-/-}$ mice. *Nat. Cell Biol.* 3:121–127.

Glouchankova, L., U.M. Krishna, B.V.L. Potter, J.R. Falck, and I. Bezprozvanny. 2000. Association of the inositol (1,4,5)-trisphosphate receptor ligand binding site with phosphatidylinositol (4,5)-bisphosphate and adenophostin A. *Mol. Cell Biol. Res. Com-*

mun. 3:153–158.
Hermosura, M.C., M.K. Monteilh-Zoller, A.M. Scharenberg, R. Penner, and A. Fleig. 2002. Dissociation of the store-operated calcium current I(CRAC) and the Mg-nucleotide-regulated metal ion current MagNuM. *J. Physiol.* 539:445–458.
Hess, P., and R.W. Tsien. 1984. Mechanism of ion permeation through calcium channels. *Nature.* 309:453–456.
Hille, B. 2001. Ionic Channels of Excitable Membranes. 3rd ed. Sinauer Associates, Sunderland, MA.
Hoth, M., and R. Penner. 1992. Depletion of intracellular calcium stores activates a calcium current in mast cells. *Nature.* 355:353–356.
Hoth, M., and R. Penner. 1993. Calcium release-activated calcium current in rat mast cells. *J. Physiol.* 465:359–386.
Irvine, R.F. 1990. "Quantal" Ca release and the control of Ca entry by inositol phosphates - a possible mechanism. *FEBS Lett.* 263:5–9.
Jackson, P.S., and K. Strange. 1995. Single-channel properties of a volume-sensitive anion conductance. Current activation occurs by abrupt switching of closed channels to an open state. *J. Gen. Physiol.* 105:643–660.
Kaznacheyeva, E., A. Zubov, K. Gusev, I. Bezprozvanny, and G.N. Mozhayeva. 2001. Activation of calcium entry in human carcinoma A431 cells by store depletion and phospholipase C-dependent mechanisms converge on ICRAC-like calcium channels. *Proc. Natl. Acad. Sci. USA.* 98:148–153.
Kaznacheyeva, E., A.N. Zubov, A. Nikolaev, V. Alexeenko, I. Bezprozvanny, and G.N. Mozhayeva. 2000. Plasma membrane calcium channels in human carcinoma A431 cells are functionally coupled to $InsP_3R$-PIP_2 complexes. *J. Biol. Chem.* 275:4561–4564.
Kerschbaum, H.H., and M.D. Cahalan. 1999. Single-channel recording of a store-operated Ca^{2+} channel in Jurkat T lymphocytes. *Science.* 283:836–839.
Kim, H.Y., D. Thomas, and M.R. Hanley. 1995. Chromatographic resolution of an intracellular calcium influx factor from thapsigargin-activated Jurkat cells. Evidence for multiple activities influencing calcium elevation in Xenopus oocytes. *J. Biol. Chem.* 270:9706–9708.
Kiselyov, K., G.A. Mignery, M.X. Zhu, and S. Muallem. 1999a. The N-terminal domain of the IP_3 receptor gates store-operated hTrp3 channels. *Mol. Cell.* 4:423–429.
Kiselyov, K., X. Xu, G. Mozhayeva, T. Kuo, I. Pessah, G. Mignery, X. Zhu, L. Birnbaumer, and S. Muallem. 1998. Functional interaction between $InsP_3$ receptors and store-operated Htrp3 channels. *Nature.* 396:478–482.
Kiselyov, K.I., A.G. Mamin, S.B. Semyonova, and G.N. Mozhayeva. 1997. Low-conductance high selective inositol (1,4,5)-trisphosphate activated Ca^{2+} channels in plasma membrane of A431 carcinoma cells. *FEBS Lett.* 407:309–312.
Kiselyov, K.I., S.B. Semyonova, A.G. Mamin, and G.N. Mozhayeva. 1999b. Miniature Ca^{2+} channels in excised plasma-membrane patches: activation by IP3. *Pflugers Arch.* 437:305–314.
Kozak, J.A., H.H. Kerschbaum, and M.D. Cahalan. 2002. Distinct properties of CRAC and MIC channels in RBL cells. *J. Gen. Physiol.* 120:221–235.
Montell, C., L. Birnbaumer, and V. Flockerzi. 2002. The TRP channels, a remarkably functional family. *Cell.* 108:595–598.
Mori, Y., M. Wakamori, T. Miyakawa, M. Hermosura, Y. Hara, M. Nishida, K. Hirose, A. Mizushima, M. Kurosaki, E. Mori, et al. 2002. Transient receptor potential 1 regulates capacitative Ca^{2+} entry and Ca^{2+} release from endoplasmic reticulum in B lymphocytes. *J. Exp. Med.* 195:673–681.
Mozhayeva, G.N., A.P. Naumov, and Y.A. Kuryshev. 1990. Inositol 1,4,5-trisphosphate activates two types of Ca^{2+}-permeable channels in human carcinoma cells. *FEBS Lett.* 277:233–234.
Nadler, M.J., M.C. Hermosura, K. Inabe, A.L. Perraud, Q. Zhu, A.J. Stokes, T. Kurosaki, J.P. Kinet, R. Penner, A.M. Scharenberg, and A. Fleig. 2001. LTRPC7 is a Mg.ATP-regulated divalent cation channel required for cell viability. *Nature.* 411:590–595.
Nilius, B., and G. Droogmans. 2001. Ion channels and their functional role in vascular endothelium. *Physiol. Rev.* 81:1415–1459.
Parekh, A.B., and R. Penner. 1997. Store depletion and calcium influx. *Physiol. Rev.* 77:901–930.
Patterson, R.L., D.B. van Rossum, and D.L. Gill. 1999. Store-operated Ca^{2+} entry: evidence for a secretion-like coupling model. *Cell.* 98:487–499.
Prakriya, M., and R.S. Lewis. 2002. Separation and characterization of currents through store-operated CRAC channels and Mg^{2+}-inhibited cation (MIC) channels. *J. Gen. Physiol.* 119:487–507.
Premack, B.A., T.V. McDonald, and P. Gardner. 1994. Activation of Ca^{2+} current in Jurkat T cells following the depletion of Ca^{2+} stores by microsomal Ca^{2+}-ATPase inhibitors. *J. Immunol.* 152: 5226–5240.
Putney, J.W., Jr., and G.S. Bird. 1993. The signal for capacitative calcium entry. *Cell.* 75:199–201.
Putney, J.W., Jr., L.M. Broad, F.J. Braun, J.P. Lievremont, and G.S. Bird. 2001. Mechanisms of capacitative calcium entry. *J. Cell Sci.* 114:2223–2229.
Randriamampita, C., and R.Y. Tsien. 1993. Emptying of intracellular Ca^{2+} stores releases a novel small messenger that stimulates Ca^{2+} influx. *Nature.* 364:809–814.
Runnels, L.W., L. Yue, and D.E. Clapham. 2001. TRP-PLIK, a bifunctional protein with kinase and ion channel activities. *Science.* 291:1043–1047.
Tang, J., Y. Lin, Z. Zhang, S. Tikunova, L. Birnbaumer, and M.X. Zhu. 2001. Identification of common binding sites for calmodulin and inositol 1,4,5-trisphosphate receptors on the carboxyl termini of trp channels. *J. Biol. Chem.* 276:21303–21310.
Trepakova, E.S., P. Csutora, D.L. Hunton, R.B. Marchase, R.A. Cohen, and V.M. Bolotina. 2000. Calcium influx factor directly activates store-operated cation channels in vascular smooth muscle cells. *J. Biol. Chem.* 275:26158–26163.
Tu, J.C., B. Xiao, J.P. Yuan, A.A. Lanahan, K. Leoffert, M. Li, D.J. Linden, and P.F. Worley. 1998. Homer binds a novel proline-rich motif and links group 1 metabotropic glutamate receptors with IP3 receptors. *Neuron.* 21:717–726.
Venkatachalam, K., D.B. van Rossum, R.L. Patterson, H.T. Ma, and D.L. Gill. 2002. The cellular and molecular basis of store-operated calcium entry. *Nat. Cell Biol.* 4:E263–E272.
Xiao, B., J.C. Tu, and P.F. Worley. 2000. Homer: a link between neural activity and glutamate receptor function. *Curr. Opin. Neurobiol.* 10:370–374.
Yao, Y., A.V. Ferrer-Montiel, M. Montal, and R.Y. Tsien. 1999. Activation of store-operated Ca^{2+} current in *Xenopus* oocytes requires SNAP-25 but not a diffusible messenger. *Cell.* 98:475–485.
Yoshikawa, F., M. Morita, T. Monkawa, T. Michikawa, T. Furuichi, and K. Mikoshiba. 1996. Mutational analysis of the ligand binding site of the inositol 1,4,5-trisphosphate receptor. *J. Biol. Chem.* 271:18277–18284.
Zitt, C., C.R. Halaszovich, and A. Luckhoff. 2002. The TRP family of cation channels: probing and advancing the concepts on receptor-activated calcium entry. *Prog. Neurobiol.* 66:243–264.
Zubov, A.I., E.V. Kaznacheyeva, A.V. Nikolaev, V.A. Alexeenko, K. Kiselyov, S. Muallem, and G.N. Mozhayeva. 1999. Regulation of the miniature plasma membrane Ca^{2+} channel I_{min} by inositol 1,4,5-trisphosphate receptors. *J. Biol. Chem.* 274:25983–25985.
Zweifach, A., and R.S. Lewis. 1993. The mitogen-regulated calcium current of T lymphocytes is activated by depletion of intracellular calcium stores. *Proc. Natl. Acad. Sci. USA.* 90:6295–6299.